Early-Late Correlation for Wideband Interference AoA Estimation and Suppression in Analog Uniformly Spaced Linear TTD Arrays

Foad Beheshti, Ruifu Li, Subhanshu Gupta, and Danijela Cabric

Abstract-Interference estimation and mitigation are of high importance in many applications of array signal processing. State-of-the-art angle and direction estimation techniques for digital arrays often rely on computationally-intensive complex algorithms. This paper introduces a novel delay measurement based low complexity Angle-of-Arrival (AoA) estimation method using analog True-Time-Delay (TTD) arrays for suppression of a single strong interference. The core of our method is the novel analog Early-Late Correlation (ELC) function that exhibits linear and odd properties enabling efficient time delay estimation with leading-lagging detections. Utilizing ELC timedelay measurements across different antenna elements in a linear TTD array, the AoA is estimated via a least-squares line-fitting solution. Interference suppression is achieved through destructive signal combining after applying proper delays in the analog domain. Simulations demonstrate the method's efficacy, achieving an interference suppression > 40dB for an OFDM interferer signal with Interference-to-Noise Ratio (INR) > -20dB and 100MHz BW in a 4-element linear TTD array.

Index Terms—Interference, Estimation, Suppression, Delay, AoA, ELC, linear TTD Arrays

I. INTRODUCTION

In wideband wireless communications systems, one of the important consideration is the ability to manage strong interferences along with weak desired signals. With the advancements of antenna array technologies, interference mitigation in wideband systems can be efficiently performed using spatial filtering based on AoA. Extensive research has been carried out on AoA estimation techniques and algorithms [1]-[13] primarily targeting digital arrays [2], [3], [9], [10] among which the most well-known and widely-used algorithms are MUSIC [14] and ESPRIT [15]. Recent research has focused on optimized techniques for hybrid arrays based on MUSIC and ESPRIT [5], [7]. Analog TTD arrays have been recently considered for wideband communications systems at millimeterwave frequencies, where novel algorithms for beam-training and interference nulling have been proposed in [6], [11], [12]. However these prior works using TTD arrays have not

This work was supported in part by NSF CAREER award (#1944688), NSF Award #1955306, and 1955672. This work was also supported in part by CDADIC.

Foad Beheshti and Subhanshu Gupta are with the School of Electrical Engineering and Computer Science, Washington State University, Pullman, WA 99164 USA (e-mail: foad.beheshti@wsu.edu).

Ruifu Li, and Danijela Cabric are with the Department of Electrical and Computer Engineering, University of California, Los Angeles, Los Angeles, CA 90095 USA (e-mail: doanr37@ucla.edu).

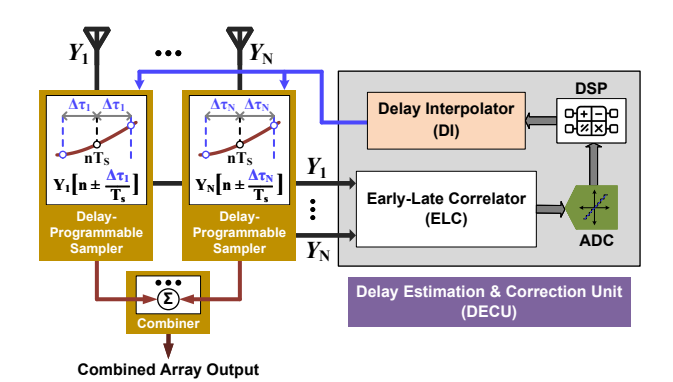


Fig. 1: Proposed Architecture

addressed and achieved high accuracy requirements needed for wideband interference suppression.

In this paper, we introduce a time-domain based AoA estimation implemented with analog delay measurements based on which the analog TTD array can suppress a single-strong interference. The approach deploys a novel ELC circuitry in analog wideband TTD arrays that enables low-complexity time-delay measurements. The proposed algorithm efficiently measures inter-element spatial delay and uses least-squares algorithm to estimate AoA based on the time-delay progression exhibited in linear uniform arrays. The new analog correlation technique, referred as ELC, computes linear odd correlation function of the delay between two signals. After the time-delay estimation, the array applies a proper TTD signal alignment in the analog domain which effectively supresses a wideband interference source.

The paper is organized as follows. Section II describes the proposed architecture and methods. The simulation results are presented in Section III. Section IV concludes the paper and describes the remaining research problems.

II. PROPOSED ARCHITECTURE AND METHODS

The proposed architecture integrates Delay Estimation and Correction Unit (DECU), shown in Fig. 1, in an *N*-element uniformly spaced linear TTD array to enable autonomous interference estimation and cancellation. DECU incorporates an ELC that captures the elements' pairwise analog correlation followed by an Analog-to-Digital Converter (ADC) to digitize the ELC output. A Digital Signal Processor (DSP) uses ADC data to estimate the inter-element delay and feeds the Delay Interpolator (DI) to properly control the Delay-Programmable

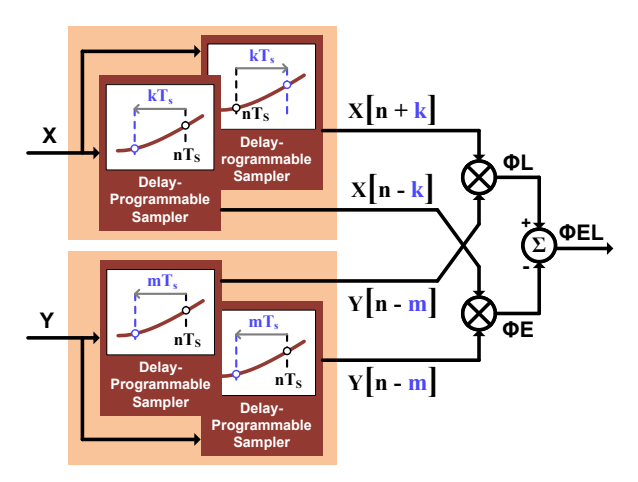


Fig. 2: ELC general implementation

Samplers in the TTD array for applying the estimated delay in the analog domain. In this approach, by sweeping a custom TTD-applied time delay in each of the elements, the proposed ELC captures the overall time delay $\Delta \tau$ between the signals from different pairs of antenna elements. This delay corresponds to the inherent spatial delay for a given AoA under uniform antenna elements spacing. The correlation data from ELC results in a correlation matrix that is used to estimate the spatial delay. The estimated spatial delay is then used to destructively combine signals from different antennas in analog domain for effective interference mitigation. It should be noted that, for the remainder of this paper, the term 'signal' refers to 'interference signal,' unless explicitly stated otherwise, to ensure brevity and simplicity.

A. ELC

The ELC circuit, shown in Fig. 2 in its general implementation, is used to compute ϕ_{EL} which is simply the subtraction of two correlation functions named as Early Correlation ϕ_E and Late Correlation ϕ_L respectively:

$$\phi E L = \phi L - \phi E \tag{1}$$

ELC is called Early-Late Cross-Correlation (ELXC) when applied on two different signals, while it is Early-Late Auto-Correlation (ELAC) when applied on a single signal. Next, we first discuss the ELXC and then ELAC emphasizing on their symmetry property as one of the two the key features of ELC for lead-lag detection exploited in this study.

1) ELXC: According to Fig. 2, we define ELXC, ϕ_{ELxy} , as the ϕ_{EL} in (1) for two finite-length signals x[n] and y[n] of same length N_s where ϕ_E and ϕ_L are two cross correlations in which the samples of the first signal x[n] is leading in the ϕ_E and lagging in the ϕ_L both by same amount k, while the samples of the second signal, e.g. y[n], is lagging in both ϕ_E and ϕ_L by same amount m:

$$\phi E L_{xy}[k, m] = \sum_{n=0}^{N_s - 1} x [n + k] y [n - m] - \sum_{n=0}^{N_s - 1} x [n - k] y [n - m]$$

where k and m are, respectively, called the Early-Late Delay (ELD) and Main Delay (MD).

Before proceeding, it is worth recalling from [16], [17] the definitions of discrete-time cross-correlation $\phi_{xy}[n]$ and auto-correlation $\phi_{yy}[n]$ functions:

$$\begin{cases}
\phi_{xy}[n] = \sum_{m=0}^{N_s - 1} x [m+n] y [m] \\
\phi_{yy}[n] = \sum_{m=0}^{N_s - 1} y [m+n] y [m]
\end{cases}$$
(3)

where x[m+n] is a circular shift of x[m], i.e.:

$$x[m+n] = x \left[m+n - \lfloor \frac{m+n}{N_s} \rfloor N_s \right]$$
 (4)

where, | | is the floor function.

According to the cross-correlation definition above, ELXC in (2) is simplified as:

$$\phi EL_{xy}[k,m] = \phi_{xy}[m+k] - \phi_{xy}[m-k] \tag{5}$$

2) *ELAC*: The definition of ELAC, ϕ_{ELyy} , is same as ϕ_{ELxy} in (2) but for same signals i.e. x[n] = y[n]:

$$\oint EL_{yy}[k,m] = \sum_{n=0}^{N_s - 1} y[n+k] y[n-m] - \sum_{n=0}^{N_s - 1} y[n-k] y[n-m]$$
(6

Similar to ELXC, ELAC equation above can be rewritten based on auto-correlation function $\phi_{uu}[n]$ (3) as below:

$$\phi EL_{yy}[k,m] = \phi_{yy}[m+k] - \phi_{yy}[m-k] \tag{7}$$

Utilizing the even property of the auto-correlation function $\phi_{yy}[-k] = \phi_{yy}[k]$ [16], most important symmetry properties of ELAC in the above equation are obtained as follows:

$$\begin{cases}
\phi E L_{yy}[-k,m] = -\phi E L_{yy}[k,m] \\
\phi E L_{yy}[k,-m] = -\phi E L_{yy}[k,m]
\end{cases}$$
(8)

where it is implied that ELAC is an odd function with respect to each of ELD and MD individually. The odd property of ELAC is its key feature that distinguishes it from conventional auto-correlation function, enabling the detection of leading and lagging signals.

We are interested in viewing ELAC from the perspective of delay as it relates to a single signal and its delayed version which is of key interest in our problem. In the next subsection, a special version of ELAC named Half-Sample ELAC (HS-ELAC) is introduced and used for the rest of the paper in which the ELD is set to 1/2 (a fractional delay) and MD is designed as a variable fractional delay.

It is worth shortly discussing the integer and fractional delays before proceeding. In discrete-time signal processing [16], [17], $x[n\pm k]$ is considered as the delayed x[n] by integer number $\pm k$. However, delay can also be a fractional delay d, i.e. $x[n\pm d]$ where 0<|d|<1. To better understand and represent the integer and fractional delays in discrete-time,

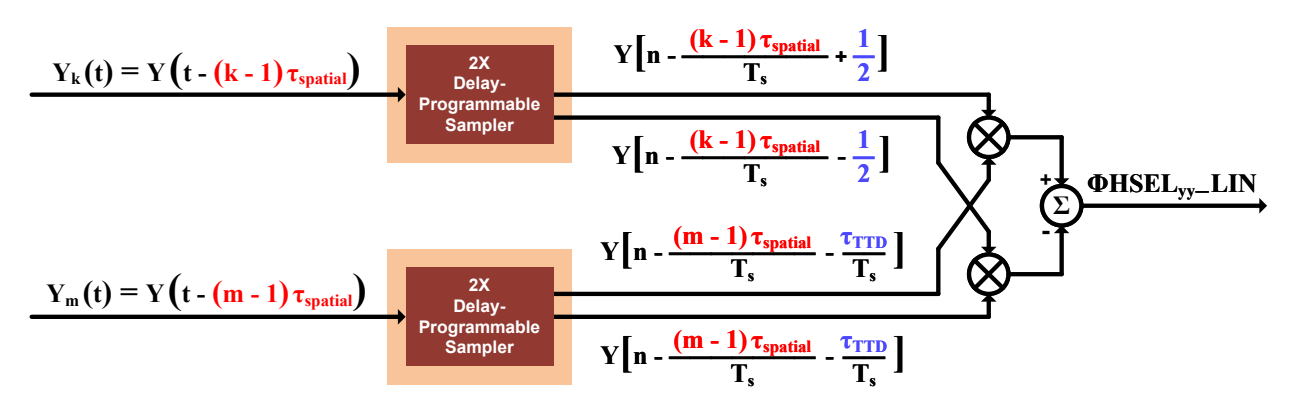


Fig. 3: HS-ELAC implemented in the linear TTD array

we consider x[n] as the sampled value of the continuous-time signal x(t) at time $t = nT_s$:

$$x[n] = x(nT_s) (9$$

where T_s is the sampling period. Considering above, the integer delay k in $x[n\pm k]=x$ $(nT_s\pm kT_s)$ indicates a time delay by integer numbers of T_s , i.e. $\pm kT_s$, and the fractional delay d in $x[n\pm d]=x$ $(nT_s\pm dT_s)$ implies a time delay by a fraction of T_s , i.e. $\pm dT_s$, which can be any amount of time smaller than T_s since 0<|d|<1. Integer and fractional delays can also be combined to represent any delay in general as $x[n\pm k\pm d]$.

Considering discrete-time signals as sampled values of continuous-time signals in (9), two scenarios for a real time delay are possible in practice including signal delay and sampling delay. Signal delay happens when y(t) is delayed in time by $\Delta \tau$, i.e. $\hat{y}(t) = y(t - \Delta \tau)$, then sampled at time $t = nT_s$; while sampling delay happens when y(t) is sampled by a time delay of $\Delta \tau$, i.e. at time $\hat{t} = nT_s - \Delta \tau$. For both delay scenarios above, the representation of an arbitrary real time delay $\Delta \tau$ in discrete-time signals using (9) is as follows:

$$\hat{y}[n] = y \left[n - \frac{\Delta \tau}{T_s} \right] = y \left[n - (k+d) \right]$$
 (10)

where $k=\lfloor \Delta \tau/T_s \rfloor$ is the integer delay and $d=\Delta \tau/T_s-\lfloor \Delta \tau/T_s \rfloor$ is the fractional delay.

B. HS-ELAC for delay estimation

High resolution time-delay estimation requires realization of a delay function with high gain, as higher gain enhances the power of the function output (that carries information about delay) against noise, allowing for improved measurement accuracy. Another important factor, especially in case of TTD linear arrays, is the ability to detect leading and lagging signals which directly imposes the odd property on the function. Taking advantage of an odd symmetry, HS-ELAC is found as a well-fit solution in a differential system for time-delay detection with positive and negative signs indicating leading and lagging signals.

As briefly mentioned before, HS-ELAC, ϕ_{HSELyy} , is a special case of ϕ_{EL} (7) that incorporates an ELD of 1/2, i.e. k=1/2 achieved by sampling delays of $\pm T_s/2$, and an MD of $\Delta \tau/T_s$, i.e. $m=\Delta \tau/T_s$ realized by a sampling delay of arbitrary real time delay $\Delta \tau$:

$$\phi HSEL_{yy} = \phi_{yy} \left[\frac{1}{2} + \frac{\Delta \tau}{T_s} \right] - \phi_{yy} \left[\frac{1}{2} - \frac{\Delta \tau}{T_s} \right]$$
 (11)

where, it is an odd function of $\Delta \tau$.

In HS-ELAC, ELD is constant while MD is representing an unknown real time delay which is meant to be estimated. The choice of k = 1/2 is mainly made to achieve a correlation function of delay with a gain very close to its ideal (highest possible) gain enabling time delay detection with high accuracy. In contrast, a straight forward option for ELD is 1, i.e. k = 1 for which the ELAC is called One-Sample ELAC (OS-ELAC). However, as shown in the following subsection, the OS-ELAC method provides very low gain compared to HS-ELAC. Other options for ELD are k < 1/2 or 1 < k that make hardware implementation of the sampling delay more complicated and power consuming [6], [18], [19], as fractional delay k = 1/2 can be realized by simply inverting the sampling clock using the well-known and straightforward inverter logic gates, whereas implementing fractional or integer delays k < 1/2 or 1 < k require highly complex and power-hungry Phase Interpolator (PI) circuitry [20], [21].

Following this subsection, we focus on the derivations of the HS-ELAC function to show its main properties including gain and oddity. For better understanding, first we discuss a simplified case followed by a more practical case.

1) Case I: single-tone: A normalized single-tone signal with a frequency of f and a sampling frequency of f_s , i.e. $y[n] = \cos\left[2\pi\left(f/f_s\right)n\right]$, is the simplest input signal waveform for which the HS-ELAC function will be derived. We utilize Nyquist and Coherent sampling techniques to simplify analysis resulting in $f/f_s = N_c/N_s$ where N_s , number of samples, is a power-of-2 integer and N_c , number of cycles, is the greatest prime number $\leq N_s/2$.

In this case, the HS-ELAC function, $\phi_{HSEL_{yy}_SIN}$, is derived from (11) as a sine-wave with respect to $\Delta \tau$ and of same frequency as the input signal:

$$\phi HSEL_{yy}_SIN = N_s \sin \left[\pi \left(\frac{N_c}{N_s} \right) \right] \sin \left[2\pi f \Delta \tau \right]$$
 (12)

where $N_s \sin\left[\pi\left(N_c/N_s\right)\right]$ is the sine-wave HS-ELAC gain $G_\phi_{HSELyy_SIN}$. Because, $N_c/N_s\approx (1/2)$ for a quite large N_s (i.e. \gg 1), the gain in (12) is close to N_s . The detailed analysis of the HS-ELAC derivation for the single-tone case has been provided in Appendix A.

It is worth mentioning here that the single-tone results in a similar function as (12) for the OS-ELAC, i.e. k=1, with only a slight deference in its gain, $G_-\phi_{OSEL_{yy}_SIN}$, where a scalar of 2 is added in the argument of the sine function making it $N_s \sin\left[2\pi\left(N_c/N_s\right)\right]$. Thus, as $N_c/N_s \approx 1/2$, $G_-\phi_{OSEL_{yy}_SIN} \ll N_s$ while $G_-\phi_{HSEL_{yy}_SIN} \approx N_s$ resulting in higher correlation.

2) Case II: Practical Case: Small delay range in wideband arrays: In practice, we are interested in wideband arrays for which the delay range is very small resulting in a delay-bandwidth product much smaller than 1, i.e. $\Delta \tau \times BW \ll 1$. In this case, if $\Delta \tau$ is small enough to satisfy $\Delta \tau / T_s < 1/2$, then we can use the following linear interpolation for simplicity:

$$\phi_{yy} \left[\frac{1}{2} \pm \frac{\Delta \tau}{T_s} \right] = \frac{(q-p) \phi_{yy} \left[\frac{1}{2} \right] + q \phi_{yy} \left[\frac{1}{2} \pm \frac{1}{2} \right]}{q}$$
 (13)

where $\Delta \tau/T_s = p/q$ while p and q are mutually prime integers. Using above linear interpolation, the HS-ELAC for any delay $\Delta \tau$ where $\Delta \tau/T_s < 1/2$ is a linear function of the delay $\phi_{HSEL_{yy}_LIN}$ derived as follows:

$$\phi HSEL_{yy}_LIN = \left(\phi_{yy}[1] - \phi_{yy}[0]\right) \left(\frac{\Delta \tau}{T_s}\right)$$
 (14)

where, the term $(\phi_{yy}[1] - \phi_{yy}[0])$ is the linear HS-ELAC gain $_{G}\phi_{HSEL_{yy}_LIN}$.

The ϕ_{HSELyy_LIN} versus $\Delta \tau$ relationship in (14) is a straight line with zero intercept making it a simple relationship for accurate time delay estimation which is the focus of this paper.

C. Spatial delay and AoA estimation using HS-ELAC in linear TTD arrays

In an N-element uniformly spaced linear array, interference signal impinging on the array from a given AoA creates a response such that each element experiences a signal delay $\tau_{spatial}$ with respect to the previous element. Accurately estimating $\tau_{spatial}$ and properly compensating for it enables wideband interference cancellation in linear TTD arrays, as we will discuss next. First, we propose a new approach for estimating $\tau_{spatial}$ utilizing the ELC circuit in linear TTD array. Then, we show how a wideband interference source can be cancelled by using the estimated spatial delay $\hat{\tau}_{spatial}$.

1) Correlation matrix: The HS-ELAC implemented in the linear TTD array as shown in Fig. 3 computes the interelement pairwise correlation (m,k) while a sampling delay of τ_{TTD} is applied via delay-programmable-samplers on the m^{th} element. For N-element array we apply HS-ELAC for all combinations of the element pairs, $1 \leq m, k \leq N$, and create a correlation matrix of size $N \times N$ as below:

$$\left[\left(\tau_{TTD}, \phi HSEL_{yy}_LIN \right)_{mk} \right]_{N \times N} \tag{15}$$

where for each (m,k) element pair the τ_{TTD} is swept across a defined range with a specific resolution. As the TTD delay is later used to apply the estimated spatial delay for interference cancellation, its range and resolution is determined based on the following considerations: range should cover the expected spatial delay based on the array geometry and resolution should be set such that the range-to-resolution ratio, determining the data points per pair measurement, is high enough to attenuate noise level through averaging.

2) Least-squares estimation: When computing the ELC correlation, TTD-applied sampling delay τ_{TTD} is added on top of the signal delay $\tau_{spatial}$. Therefore, the overall delay between the element pair (m,k) is:

$$\Delta \tau(m,k) = \tau_{TTD} + (m-k)\,\tau_{spatial} \tag{16}$$

where (m-k) scales the spatial delay between the element pair based on their location in the linear array.

Given the above delay relationship and considering the linear HS-ELAC function (14), the data points described in (15) should satisfy the following:

$$\phi HSEL_{yy}_LIN = \frac{G_\phi HSEL_{yy}_LIN}{T_s} \left[\tau_{TTD} + (m-k) \tau_{spatial} \right]$$
 (17)

We note that the captured correlation matrix data (15) can be fitted to a straight line that depends on $\tau_{spatial}$.

Using the well-known Least-Square approach, we can solve the line-fitting equation (17) for finding the $\hat{\tau}_{spatial}$ as follows:

$$\hat{\tau}_{spatial} = \frac{\left(\sum \phi HSEL_{yy_LIN}\right) \left[N\sum \tau_{TTD}^2 - \left(\sum \tau_{TTD}\right)^2\right]}{N\left[N\sum \tau_{TTD}\phi HSEL_{yy_LIN} - \left(\sum \tau_{TTD}\right) \left(\sum \phi HSEL_{yy_LIN}\right)\right]_{(18)}}$$

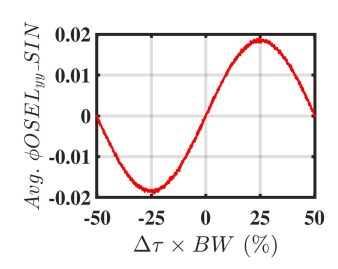
Using $\hat{\tau}_{spatial}$ above, AoA can be indirectly recovered as below:

$$\hat{AoA} = \arcsin\left(\frac{c \ \hat{\tau}_{spatial}}{d}\right) \tag{19}$$

where d is the linear array uniform spacing and c is the light speed in free air.

D. Interference cancellation with TTD alignment

In order for the interference to get suppressed, the interference signals received at the antenna elements should be time-aligned and then destructively combined. The time alignment is realized by inserting a TTD-applied sampling delay of $\hat{\tau}_{spatial}$ on the leading signal in a set of two neighboring elements. We first discuss TTD alignment using



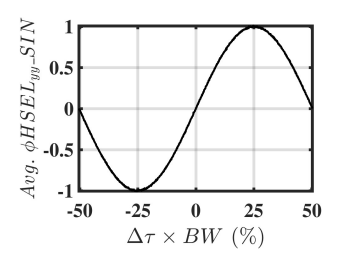


Fig. 4: Averaged ϕ_{OSELyy_SIN} (Left) and ϕ_{HSELyy_SIN} (Right) versus $\Delta \tau$ for normalized single-tone signal with $f=99.414 \mathrm{MHz}$, $f_s=200 \mathrm{MHz}$, and $INR=10 \mathrm{dB}$.

 $\hat{\tau}_{spatial}$ and then focus on the destructive combination for suppression.

1) TTD alignment: In order to coherently align signals from all elements in time, a TTD-applied sampling delay of $(N-i)\,\hat{\tau}_{spatial}$ is added to the i^{th} element which in addition to signal delay of $(i-1)\tau_{spatial}$ results in the following signal at the antenna element i^{th} element:

$$\hat{y}_{i}[n] = y \left[n - (i-1) \left(\frac{\tau_{spatial}}{T_{s}} \right) - (N-i) \left(\frac{\hat{\tau}_{spatial}}{T_{s}} \right) \right]$$
 (20)

Considering a delay estimation error of τ_{err} for the estimated spatial delay $\hat{\tau}_{spatial}$, i.e. $\hat{\tau}_{spatial} = \tau_{spatial} + \tau_{err}$, simplifies the above equation as follows:

$$\hat{y}_i[n] = y \left[n - (N - 1) \left(\frac{\tau_{spatial}}{T_s} \right) - (N - i) \left(\frac{\tau_{err}}{T_s} \right) \right] \quad (21)$$

Before proceeding, it is worth translating the time-alignment equation above written in time-domain to the frequency-domain using Discrete Fourier Transform (DFT) to simplify the remaining analysis. Therefore, the N_s -point DFT of the TTD-aligned signal of i^{th} element (21) is as follows:

$$\hat{Y}_{i}[k] = e^{-j\left(\frac{2\pi}{N_{s}}\right)k\left[(N-1)\left(\frac{\tau_{spatial}}{T_{s}}\right) + (N-i)\left(\frac{\tau_{err}}{T_{s}}\right)\right]}Y[k]$$
 (22)

where N_s is also the length of signal samples.

For the remainder of this section, we will do the analysis in frequency-domain.

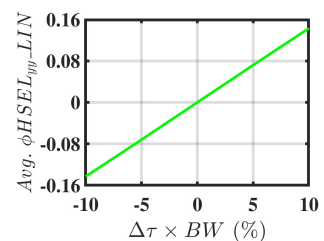
2) Destructive combination: The first solution for destructive combination after time-alignment is to simply subtract the signal of every other element from that of the previous one. Thus, the first destructively combined signal $\hat{Y}_{(1)}[k]$ can be represented in the frequency-domain as follows:

$$\hat{Y}_{(1)}[k] = \left[(-1)^{i-1} \right]_{1 \times N} \times \left[\hat{Y}_{i}[k] \right]_{N \times 1}$$
(23)

Using (22) and (23) the first beam-nulling gain $|G_{BN(1)}[k]|$ can be obtained as follows:

$$\left| G_{BN(1)}[k] \right| = \left| \frac{\hat{Y}_{(1)}[k]}{Y[k]} \right| = \left| \sum_{i=1}^{N} (-1)^{i-1} e^{\left[j \left(\frac{2\pi}{N_s} \right) k \left(\frac{T_{err}}{T_s} \right) \right] i} \right|$$
 (24)

In general, destructive combination can happen when half of the channels' signals are subtracted from those of the other



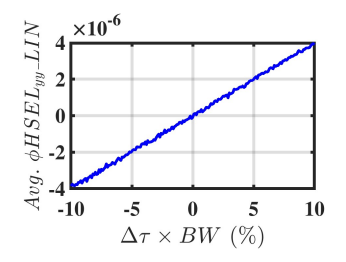


Fig. 5: Averaged $\phi_{HSEL_{yy}_LIN}$ functions for two different normalized signals both with INR = 0 dB. Left: two-tone signal at frequencies $f_1 = 31.2 MHz$ and $f_2 = 89.2 MHz$ sampled at $f_s = 500 \text{MHz}$. Right: OFDM signal with parameters mentioned in TABLE II.

half. Additionally, the scalar of the error term in (24), i.e. $[j\ (2\pi/N_s)\ k\ (1/T_s)]\ i$, is dependent on the element position in the row i, implying different beam-nulling gains for different destructive combinations. Therefore, $\binom{N-1}{N/2}$ unique destructive combinations in an N-element array, forming Truncated Hadamard Matrix (THM) [22], result in different beam-nulling gains. Thus, similar to (23), all possible destructively combined signals using THM are expressed as below:

$$\left[\hat{Y}_{(m)}[k]\right]_{M\times 1} = \left[THM_{mi}\right]_{M\times N} \times \left[\hat{Y}_{i}[k]\right]_{N\times 1} \tag{25}$$

where, $1 \le m \le M = \binom{N-1}{N/2}$ and THM_{mi} is the (m,i)-th element of the THM.

Similar to (24) and using (22) and (25), different beamnulling gains $|G_{BN(m)}[k]|$ are derived as below:

$$\left[\left|G_{BN(m)}[k]\right|\right]_{M\times 1} = \left[\left|\sum_{i=1}^{N} THM_{mi} e^{\left[j\left(\frac{2\pi}{N_{S}}\right)k\left(\frac{T_{err}}{T_{S}}\right)\right]i}\right|\right]_{M\times 1}$$
(26)

As shown in previous studies [23], [24], Although different, multiple beam-nulling gains lead to slightly different gains for the target interference AoA even if ideally the array steers toward the interference with no error. Given this fact, the choice of THM mainly depends on the beam-nulling gain at the desired signal AoA which is assumed different than interference AoA. As in this paper the focus is solely on the interference AoA, we pursue interference cancellation using only the first beam-nulling gain $|G_{BN(1)}[k]|$.

III. SIMULATION RESULTS

This section presents simulation results to illustrate the performance of the ELC algorithm in spatial delay estimation and interference cancellation. Unless stated otherwise, the following parameters are used for all simulations:

BW	N_s	TTD Resolution	TTD Range
100MHz	1024	2ps	[-1ns, 1ns]

TABLE I: Simulation Parameters

Fig. 4 shows the averaged ϕ_{OSELyy_SIN} and ϕ_{HSELyy_SIN} functions where $f=99.414 \mathrm{MHz}$ and $f_s=200 \mathrm{MHz}$ satisfying Nyquist and Coherent sampling conditions for the normalized single-tone signal with a INR of

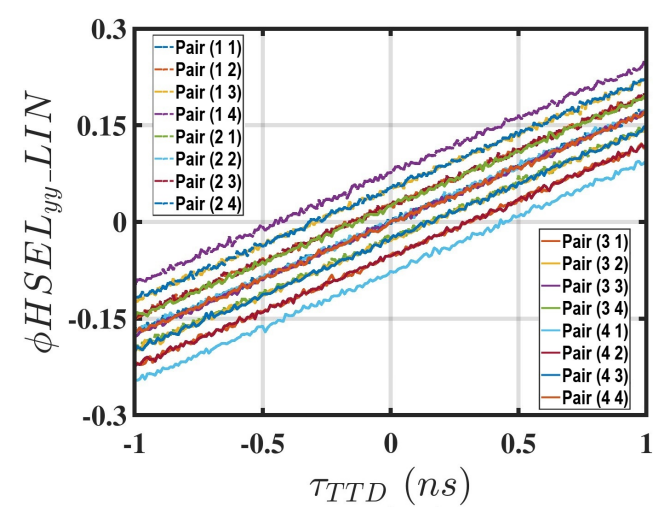


Fig. 6: ϕ_{HSELyy_LIN} in linear 4-element TTD array for an OFDM signal with INR = 0 dB and parameters mentioned in TABLE II.

10dB. As the analysis in Section II.B demonstrated, averaged $G_\phi HSEL_{yy}_SIN$ is unity while averaged $G_\phi OSEL_{yy}_SIN$ is approximately 0.02 which is much smaller than 1. As it is obvious in Fig. 4, the higher gain of HS-ELAC compared to OS-ELAC makes it more resilient to noise, resulting in improved estimation accuracy when used for time delay detection.

Shown in Fig. 5 is the averaged $\phi_{HSEL_{yy}_LIN}$ functions applied on two different normalized signals both with $INR=0 {\rm dB}$; for the left graph, signal is a two-tone at frequencies $f_1=31.2MHz$ and $f_2=89.2MHz$ sampled at $f_s=500 {\rm MHz}$ while for right graph, an OFDM signal with following parameters is used:

symbols	modulation	sub-carriers	spacing
2	16-QAM	3276	30kHz

TABLE II: OFDM signal parameters

While the small range of $\Delta \tau$ in Fig. 5 guarantees the zero-crossing straight line behavior of HS-ELAC as a straightforward delay estimation for both two-tone and OFDM signals, the lower correlation exhibited in OFDM implies a higher time delay estimation error for this signal.

Fig 6 shows the performance of the proposed method for an OFDM signal with $INR=0 \mathrm{dB}$ and parameters mentioned in TABLE II in a 4-element linear array with uniform spacing 90mm leading to $\tau_{spatial}=150ps$ at $AoA=30^\circ$. Since the total delay in this case is $\Delta \tau = \tau_{TTD} + (m-n)\,\tau_{spatial}$, we can see that when $m \neq n$ the zero-crossing straight line is shifted left or right as much as $(m-n)\,\tau_{spatial}$ implying that horizontal spacing between two neighboring lines is equal to $\tau_{spatial}$. The data points of the line associated with the (m,k) element pair in this figure form its corresponding element in the correlation matrix described in Section II.C.

Result of Fig. 6 is used for estimating $\tau_{spatial}=150ps$ based on the linear least-squares technique for straight line fitting. The Root Mean Square Error (RMSE) of $\hat{\tau}_{spatial}$ using this approach for OFDM signal with different INRs

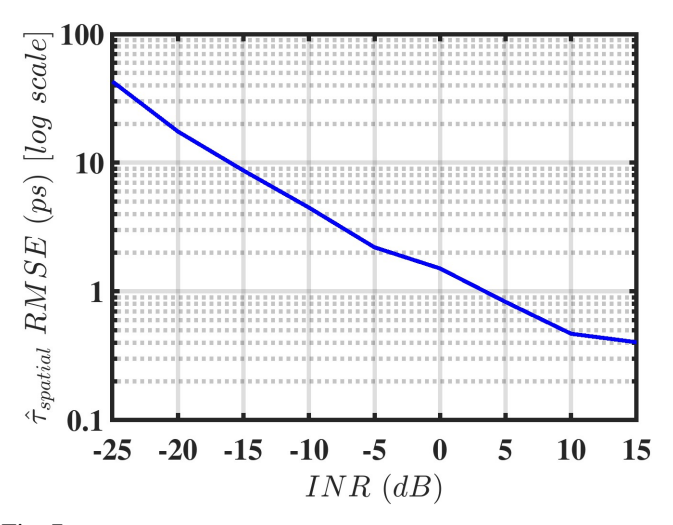


Fig. 7: Delay estimation RMSE for $\tau_{spatial} = 150ps$ across different INRs for OFDM signal with parameters mentioned in TABLE II.

is shown in Fig. 7. According to this result, the proposed method estimates the $\tau_{spatial} = 150ps$ with an RMSE < 18psfor OFDM signal with INR > -20dB which is equivalent to a relative estimation error < 12% indicating very high time-delay estimation accuracy. Using the $\hat{ au}_{spatial}$ obtained from result shown in Fig. 7, the interference signal can be suppressed in the linear array with proper time alignment followed by destructive combination. Fig 8 shows the INR of the suppressed interference with time-alignment using $\hat{ au}_{spatial}$ and without time alignment (i.e. only destructive combination) along with the INR of the interference itself while no suppression is applied. As can be observed in this figure, while destructive combination without time alignment only result in an attenuated interferer, our approach successfully mitigates the interference by lowering down its power more than 60dB below noise level for original INR > -20dB. This result shows a suppression > 40dB for OFDM signal with INR > -20dB implying high interference suppression level with the ELC technique.

IV. CONCLUSIONS AND FUTURE WORKS

In this work, we present a novel time-delay detection based approach for AoA estimation and suppression of a single wideband interferer in linear TTD arrays. Benefiting from linear and odd properties of correlation, an analog correlator ELC system architecture has been modeled that exhibits a linear function of the time-delay between two signals, and provides the delay polarity indicating leading and lagging signals. The ELC computations, enabled by controlling the TTD delays, for different antenna element pairs in a wideband linear TTD array is derived as a correlation matrix and fitted into a linear function. The inter-element spatial delay of the linear array was estimated by solving the line fitting problem with least-squares approach. The estimated spatial delay was used for time alignment enabled by TTD circuits followed by destructive combination to perform interference suppression. Simulation results demonstrate the efficacy of this approach,

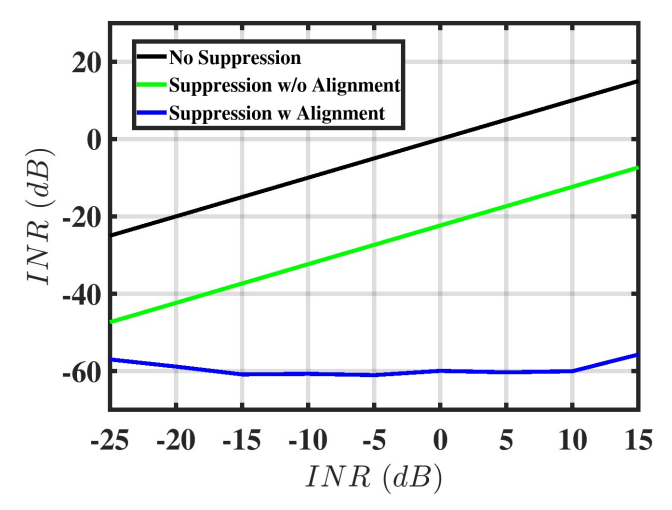


Fig. 8: Suppressed INR vs. raw INR waveform for OFDM signal with parameters mentioned in TABLE II in three conditions including: no suppression i.e. no time alignment and no destructive combination shown in black, suppression without time alignment and only with destructive combination shown in green and finally suppression with time alignment using $\hat{\tau}_{spatial}$ and destructive combination shown in blue.

achieving a time-delay estimation accuracy with an RMSE < 18ps (equivalent to a relative error < 12%) and interference suppression > 40dB for an OFDM signal with 100MHz bandwidth and INR > -20dB. Future work will explore extending this method to multi-source systems involving the cancellation of multiple interference signals.

ACKNOWLEDGMENT

The authors greatly acknowledge Praveen Kumar Venkatachala, Principal Electrical Engineer at Skyworks Solutions, Inc., for providing valuable insights that contributed to the foundation of this study. Also, the authors acknowledge support from the rest of SOCLAB and CORES lab members.

APPENDIX A DERIVATION OF HS-ELAC FUNCTION (12) FOR SINGLE TONE

Using the single tone sinusoid $y[n] = \cos \left[2\pi \left(f/f_s \right) n \right]$ where $f/f_s = N_c/N_s$, mentioned in Section II.B, as the input signal, we can start deriving $\phi_{HSEL_{yy}_SIN}$ from (11) as below:

$$\phi_{HSEL_{yy}_SIN} = \phi_{yy} \left[\frac{1}{2} + \frac{\Delta \tau}{T_s} \right] \left| -\phi_{yy} \left[\frac{1}{2} - \frac{\Delta \tau}{T_s} \right] \right|_{y=0.05}$$

Taking advantage of the ELAC original definition (6) while k=1/2 and $m=\Delta \tau/T_s$, the above equation for ϕ_{HSELyy_SIN} is rewritten as follows:

$$\begin{split} \phi HSEL_{yy}_SIN &= \\ \sum_{n=0}^{N_s-1} \cos \left[2\pi \left(\frac{N_c}{N_s} \right) \left(n + \frac{1}{2} \right) \right] \cos \left[2\pi \left(\frac{N_c}{N_s} \right) \left(n - \frac{\Delta \tau}{T_s} \right) \right] \\ &- \sum_{n=0}^{N_s-1} \cos \left[2\pi \left(\frac{N_c}{N_s} \right) \left(n - \frac{1}{2} \right) \right] \cos \left[2\pi \left(\frac{N_c}{N_s} \right) \left(n - \frac{\Delta \tau}{T_s} \right) \right] \end{split}$$

$$\begin{split} &= \sum_{n=0}^{N_s-1} \left\{ \left(\cos \left[2\pi \left(\frac{N_c}{N_s} \right) \left(n + \frac{1}{2} \right) \right] - \cos \left[2\pi \left(\frac{N_c}{N_s} \right) \left(n - \frac{1}{2} \right) \right] \right) \times \\ &\cos \left[2\pi \left(\frac{N_c}{N_s} \right) \left(n - \frac{\Delta \tau}{T_s} \right) \right] \right\} \\ &= \sum_{n=0}^{N_s-1} \left\{ 2 \sin \left[\pi \left(\frac{N_c}{N_s} \right) \right] \sin \left[2\pi \left(\frac{N_c}{N_s} \right) n \right] \times \\ &\left(\cos \left[2\pi \left(\frac{N_c}{N_s} \right) n \right] \cos \left[2\pi f \Delta \tau \right] + \sin \left[2\pi \left(\frac{N_c}{N_s} \right) n \right] \sin \left[2\pi f \Delta \tau \right] \right) \right\} \\ &= \sin \left[\pi \left(\frac{N_c}{N_s} \right) \right] \sum_{n=0}^{N_s-1} \left\{ \left(2 \sin \left[2\pi \left(\frac{N_c}{N_s} \right) n \right] \cos \left[2\pi \left(\frac{N_c}{N_s} \right) n \right] \right) \times \\ &\cos \left[2\pi f \Delta \tau \right] + \left(2 \sin^2 \left[2\pi \left(\frac{N_c}{N_s} \right) n \right] \right) \sin \left[2\pi f \Delta \tau \right] \right\} \\ &= \sin \left[\pi \left(\frac{N_c}{N_s} \right) \right] \sum_{n=0}^{N_s-1} \left\{ \sin \left[4\pi \left(\frac{N_c}{N_s} \right) n \right] \cos \left[2\pi f \Delta \tau \right] + \\ &\left(1 - \cos \left[4\pi \left(\frac{N_c}{N_s} \right) n \right] \right) \sin \left[2\pi f \Delta \tau \right] \right\} \\ &= \sin \left[\pi \left(\frac{N_c}{N_s} \right) \right] \left\{ \sum_{n=0}^{N_s-1} \sin \left[2\pi f \Delta \tau \right] + \sum_{n=0}^{N_s-1} \left(\sin \left[4\pi \left(\frac{N_c}{N_s} \right) n - 2\pi f \Delta \tau \right] \right) \right\} \\ &= \sin \left[\pi \left(\frac{N_c}{N_s} \right) \right] \left(N_s \sin \left[2\pi f \Delta \tau \right] + \sum_{n=0}^{N_s-1} \sin \left[4\pi \left(\frac{N_c}{N_s} \right) n - 2\pi f \Delta \tau \right] \right) \right\} \end{split}$$

Representing the above summand as s(n), we have:

$$\phi HSEL_{yy}_SIN = \sin \left[\pi \left(\frac{N_c}{N_s}\right)\right] \left(N_s \sin \left[2\pi f \Delta \tau\right] + \sum_{n=0}^{N_s - 1} s(n)\right)$$
(27)

Using symmetry properties of sin function, it can be easily shown for the summand s(n) that the $\left(\frac{N_s}{2}+m\right)-th$ term is equal to the m-th term i.e. $s\left(\frac{N_s}{2}+m\right)=s\left(m\right)$. Then, using this property of the summand s(n) we will rewrite the sum in (27) as below:

$$\sum_{n=0}^{N_s-1} s(n) = \sum_{m=0}^{\frac{N_s}{2}-1} \left\{ s(m) + s\left(\frac{N_s}{2} + m\right) \right\} = 2 \sum_{m=0}^{\frac{N_s}{2}-1} s(m)$$

Similarly, for the summand s(m) above we have $s\left(\frac{N_s}{4}+k\right)=-s\left(k\right)$ that makes it equal to zero:

$$\sum_{m=0}^{\frac{N_s}{2}-1} s(m) = \sum_{k=0}^{\frac{N_s}{4}-1} \left\{ s(k) + s\left(\frac{N_s}{4} + k\right) \right\} = 0$$

Finally, having the sum in (27) equal to zero yields the following for $\phi_{HSEL_{yy}_SIN}$:

$$\phi_{HSEL_{yy}_SIN} = N_s \sin \left[\pi \left(\frac{N_c}{N_s} \right) \right] \sin \left[2\pi f \Delta \tau \right]$$

Thus, the derivation is now complete.

REFERENCES

 O. A. Oumar, M. F. Siyau, and T. P. Sattar, "Comparison between MU-SIC and ESPRIT direction of arrival estimation algorithms for wireless communication systems," in 1st Intl. Conf. on Future Generation Comm. Tech., 2012, pp. 99–103.

- [2] A. Badawy, T. Khattab, D. Trinchero, T. ElFouly, and A. Mohamed, "A simple angle of arrival estimation system," in *IEEE Wir. Comm. and Netw. Conf. (WCNC)*, 2017, pp. 1–6.
- [3] J. Tranter, N. D. Sidiropoulos, X. Fu, and A. Swami, "Fast unit-modulus least squares with applications in beamforming," *IEEE Trans. on Sig. Proc.*, vol. 65, no. 11, pp. 2875–2887, 2017.
- [4] G. Zhu, K. Huang, V. K. N. Lau, B. Xia, X. Li, and S. Zhang, "Hybrid beamforming via the Kronecker decomposition for the millimeter-wave massive MIMO systems," *IEEE J. on Sel. Areas in Comm.*, vol. 35, no. 9, pp. 2097–2114, 2017.
- [5] W. Liu, Y. Li, F. Yang, L. Ding, and C. Zhi, "Millimeter-wave channel estimation with interference cancellation and DOA estimation in hybrid massive MIMO systems," in 9th Intl.Conf.onWir.Comm.andSig.Proc.(WCSP), 2017, pp.1-6.
- [6] V. Boljanovic, H. Yan, C.-C. Lin, S. Mohapatra, D. Heo, S. Gupta, and D. Cabric, "Fast beam training with true-time-delay arrays in wideband millimeter-wave systems," *IEEE Transactions on Circuits and Systems* 1: Regular Papers, vol. 68, no. 4, pp. 1727–1739, 2021.
- [7] H.-T. Sheng and W.-R. Wu, "Blind AoA estimation with hybrid antenna arrays," *IEEE Trans. on Wir. Comm.*, vol. 20, no. 8, pp. 5058–5070, 2021.
- [8] M. A. Alaei, S. Golabighezelahmad, P.-T. de Boer, F. E. van Vliet, E. A. M. Klumperink, and A. B. J. Kokkeler, "Interference mitigation by adaptive analog spatial filtering for MIMO receivers," *IEEE Trans.* on Micro. Theo. and Tech., vol. 69, no. 9, pp. 4169–4179, 2021.
- [9] Z. Dai, Y. He, V. Tran, N. Trigoni, and A. Markham, "DeepAoANet: Learning angle of arrival from software defined radios with deep neural networks," *IEEE Access*, vol. 10, pp. 3164–3176, 2022.
- [10] D. Peña-Colaiocco, C.-H. Huang, K.-D. Chu, J. C. Rudell, and V. Sathe, "An optimal digital beamformer for mm-wave phased arrays with 660MHz instantaneous bandwidth in 28nm CMOS," in *IEEE Intl. Solid-State Cir. Conf. (ISSCC)*, vol. 65, 2022, pp. 1–3.
- [11] V. Boljanovic and D. Cabric, "Joint single-shot AoD/AoA estimation in mmW systems and analysis under hardware impairments," in *IEEE Intl. Conf. on Comm.*, 2023, pp. 2766–2772.
- [12] A. Wadaskar, S. Sarkar, and D. Cabric, "Millimeter wave spectrum sharing using analog true time delay array based wideband nulling," in *IEEE Intl. Symp. on Dyn. Spec. Acc. Netw. (DySPAN)*, 2024, pp. 374–382.
- [13] C. Collmann, A. B. Martinez, A. Nimr, and G. Fettweis, "Angle-of-Departure estimation algorithms for true-time-delay antenna arrays with software-defined radio," in *IEEE 4th Intl. Symp. on Joint Comm. Sens.* (JC&S), 2024, pp. 1–6.
- [14] R. Schmidt, "Multiple emitter location and signal parameter estimation," *IEEE Trans. on Ant. and Prop.*, vol. 34, no. 3, pp. 276–280, 1986.
- [15] R. Roy and T. Kailath, "ESPRIT-estimation of signal parameters via rotational invariance techniques," *IEEE Trans. on Acoustics, Speech, and Sig. Proc.*, vol. 37, no. 7, pp. 984–995, 1989.
- [16] A. V. Oppenheim, A. S. Willsky, and S. H. Nawab, Signals and systems. Prentice Hall, 1996.
- [17] A. V. Oppenheim and S. R. W., Discrete-time signal processing. Pearson Education India, 1999.
- [18] Q. Xu, C.-C. Lin, A. Wadaskar, H. Hu, D. Cabric, and S. Gupta, "A 10ns delay range 1.5ghz bw true-time-delay array-based passive-active signal combiner with negative-cap stabilized ramp for fast precise localization," in 2024 IEEE Radio Frequency Integrated Circuits Symposium (RFIC), 2024, pp. 227–230.
- [19] A. Slater, H. Abbasi, S. Poolakkal, F. Beheshti, and S. Gupta, "Enhancing continuous beam angle resolution for next generation wireless systems: A multi-stage phase-shifting polyphase filters approach," *IEEE Trans. on Cir. and Syst. I: Reg. Pap.*, vol. 71, no. 11, pp. 5200–5210, 2024
- [20] E. Ghaderi, A. Sivadhasan Ramani, A. A. Rahimi, D. Heo, S. Shekhar, and S. Gupta, "An integrated discrete-time delay-compensating technique for large-array beamformers," *IEEE Transactions on Circuits and Systems I: Regular Papers*, vol. 66, no. 9, pp. 3296–3306, 2019.
- [21] S. Mohapatra, C.-C. Lin, S. Gupta, and D. Heo, "Low-power process and temperature-invariant constant slope-and-swing ramp-based phase interpolator," *IEEE Journal of Solid-State Circuits*, vol. 58, no. 8, pp. 2267–2277, 2023.
- [22] W. Pratt, J. Kane, and H. Andrews, "Hadamard transform image coding," Proc. of the IEEE, vol. 57, no. 1, pp. 58–68, 1969.

- [23] E. Ghaderi, A. S. Ramani, A. A. Rahimi, D. Heo, S. Shekhar, and S. Gupta, "Four-element wide modulated bandwidth mimo receiver with ¿35-db interference cancellation," *IEEE Transactions on Microwave Theory and Techniques*, vol. 68, no. 9, pp. 3930–3941, 2020.
- [24] E. Ghaderi, "Analog/mixed-signal spatial signal processing for wideband multi-antenna receivers," PhD Dissertation, Washington State University, 2020